

Article

Partial Oxidation (“Aging”) and Surface Modification Decrease the Toxicity of Nanosized Zerovalent Iron

Tanapon Phenrat, Thomas C. Long, Gregory V. Lowry, and Bellina Veronesi

Environ. Sci. Technol., **2009**, 43 (1), 195-200 • DOI: 10.1021/es801955n • Publication Date (Web): 26 November 2008

Downloaded from <http://pubs.acs.org> on January 2, 2009

More About This Article

Additional resources and features associated with this article are available within the HTML version:

- Supporting Information
- Access to high resolution figures
- Links to articles and content related to this article
- Copyright permission to reproduce figures and/or text from this article

[View the Full Text HTML](#)



ACS Publications
High quality. High impact.

Partial Oxidation (“Aging”) and Surface Modification Decrease the Toxicity of Nanosized Zerovalent Iron

TANAPON PHENRAT,^{†,§}
 THOMAS C. LONG,^{#,†}
 GREGORY V. LOWRY,^{†,§} AND
 BELLINA VERONESI^{*,||}

Department of Civil and Environmental Engineering,
 Carnegie Mellon University, Pittsburgh, Pennsylvania 15213,
 Department of Environmental Sciences and Engineering,
 School of Public Health, University of North Carolina, Chapel
 Hill, North Carolina 27599-7431, Center for Environmental
 Implications of NanoTechnology (CEINT), Pittsburgh,
 Pennsylvania 15213, and National Health and Environmental
 Effects Research Laboratory, U.S. Environmental Protection
 Agency, Research Triangle Park, North Carolina 27711

Received July 15, 2008. Revised manuscript received
 October 22, 2008. Accepted October 23, 2008.

Nanoscale zero-valent iron (nZVI) is a “redox”-active nanomaterial used in the remediation of contaminated groundwater. To assess the effect of “aging” and surface modification on its potential neurotoxicity, cultured rodent microglia (BV2) and neurons (N27) were exposed to fresh nZVI, “aged” (>11 months) nZVI, magnetite, and polyaspartate surface-modified (SM) nZVI. Increases in various measures of oxidative stress indicated that BV2 microglia responded to these materials in the following rank order: nZVI > “aged” nZVI > magnetite = SM nZVI. Fresh nZVI produced morphological evidence of mitochondrial swelling and apoptosis. In N27 neurons, ATP levels were reduced in the following rank order: nZVI > SM-nZVI > “aged” nZVI = magnetite. Ultrastructurally, nZVI produced a perinuclear floccular material and cytoplasmic granularity. Both SM-nZVI produced intracellular deposits of nanosize particles in the N27. The physicochemical properties of each material, measured under exposure conditions, indicated that all had electronegative zeta potentials. The iron content of nZVI (~35%) and SM-nZVI (~25%) indicated high “redox” activity while that of “aged” and magnetite was negligible. Sedimentation and agglomeration occurred in the following rank order: nZVI > “aged” nZVI > magnetite ≫ SM-nZVI. Correlating these properties with toxicity indicated that partial or complete oxidation of nZVI reduced its “redox” activity, agglomeration, sedimentation rate, and toxicity to mammalian cells. Surface modification decreased nZVI toxicity by reducing sedimentation which limited particle exposure to the cells.

* Corresponding author phone: (919) 541-5780; fax: (919) 541-4849; e-mail: veronesi.bellina@epa.gov.

[†] Carnegie Mellon University.

[‡] University of North Carolina.

[§] Center for Environmental Implications of NanoTechnology.

^{||} U.S. Environmental Protection Agency.

[#] Present address: National Center for Environmental Assessment; US Environmental Protection Agency, Research Triangle Park, NC, 27711.

Introduction

Nanoscale zerovalent iron (nZVI) is used for the in situ remediation of groundwater pollutants (1) such as chlorinated organics (2–4) pesticides (5), and heavy metals (6, 7). Because of its larger specific surface area, higher surface reactivity (6), and unique catalytic activity (8), nZVI degrades or reduces contaminants at a faster rate than microscale ZVI (iron filings) (2). nZVI is highly “redox” active and generates reactive oxygen species (ROS) through Fenton chemistry (9). It acts as an electron donor to reduce chlorinated organic contaminants and heavy metals, rendering them less mobile. In aqueous environments, nZVI oxidizes over time (i.e., “ages”) to magnetite (Fe₃O₄), maghemite, and other iron-oxides such as hematite and goethite. For in situ applications, highly concentrated (~10 g/L) aqueous slurries of nZVI are injected directly into the ground at, or near, the source of contamination (10, 11). nZVI particles rapidly agglomerate due to magnetic forces (12, 13) and the mobility of bare nZVI is limited (few centimeters) (14). Thus nZVI is surface-modified (SM) with polymers or surfactants to increase its migration and therefore proximity to the pollutant materials (12, 14–19). The enhanced mobility of surface-modified particles and nZVI’s direct application to groundwater increase the likelihood that these materials can disperse in the environment and raise the possibility that they could enter aquifers in low concentrations and impact ecological and higher order biological systems through drinking water.

Several studies indicate that ingested or inhaled nanoparticles can cross biological barriers (i.e., alveolar, intestinal, dermal) and migrate in small numbers to various organs and tissues (20, 21) where they can potentially damage organ systems particularly sensitive to oxidative stress (OS), such as the brain. In the brain, OS is mediated by the microglia, a macrophage-like, phagocytic cell (22, 23). Upon contact with a foreign substance, the microglia elaborate cytoplasmic projections which engulf and sequester the foreign material (i.e., phagocytosis). Microglia then express the “oxidative burst” which produces multiple ROS that destroy the foreign substance through OS-mediated damage. To examine the possibility that nZVI or its related materials could produce OS-mediated neurotoxicity, rodent brain cells (BV2 microglia and N27 neurons) were tested. BV2 cells are immortalized mouse microglia that retain normal morphological and functional properties and respond to pharmaceutical agents, nanoparticles, and environmental chemicals with characteristic signs of OS (24–27). N27 are immortalized rat dopaminergic neurons dissociated from the mesencephalic cortex (28). Recent data (29) using both cell types have been used to predict OS-mediated brain damage associated with particular matter (30). These cells were exposed to nZVI materials currently used in groundwater remediation and most likely to show actual environmental risk. These included nZVI from fresh slurry, its oxidized forms (“aged”, magnetite) and fresh nZVI that had been surface-modified with sodium polyaspartate (SM-nZVI). Because of their potential “redox” activity, several major events in the cell’s OS response (e.g., oxidative burst, mitochondrial depolarization, caspase 3/7 activity) and viability (e.g., ATP reductions) were measured with various fluorescent assays. The size distribution (aggregate versus individual particles), zeta potential, and sedimentation profile of these materials were measured under exposure conditions and correlated with their cellular response. This allowed us to test the hypothesis that the physical properties of nanoparticles determine their interaction with biological systems. We proposed that the oxidative

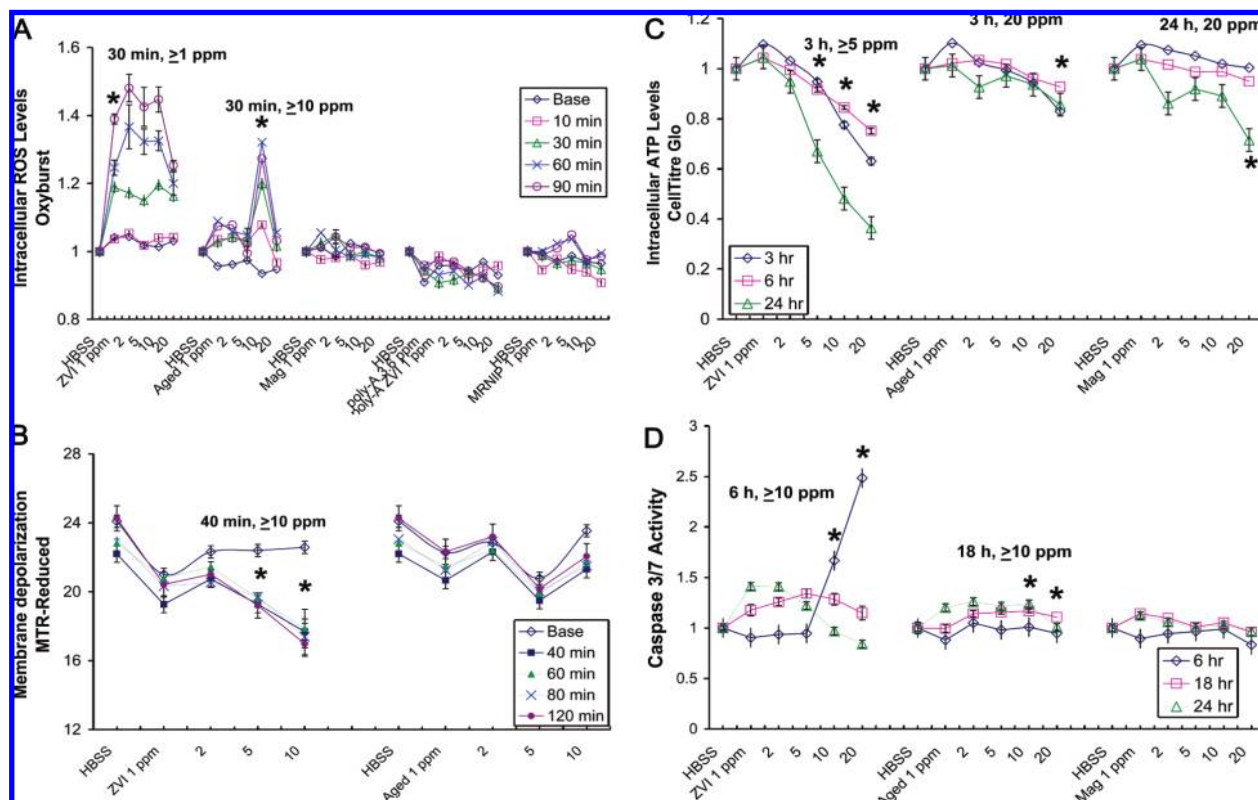


FIGURE 1. (A) BV2 microglia were incubated (30 min, 37 °C) in 10 $\mu\text{g}/\text{mL}$ Oxyburst Green in Hanks basic salt solution (HBSS) and exposed to 1–20 ppm nZVI (fresh, “aged”), magnetite, or either SM-nZVI (polyAA-nZVI and MRNIP). Significant release of ROS first occurred after 30 min in response to fresh nZVI (≥ 1 ppm) and “aged” nZVI (≥ 10 ppm). No significant release was observed for magnetite or SM-nZVI over the subsequent 90 min recording period. (B) BV2 cells were incubated with 25 nM MitoTracker Red (30 min, 37 °C). Depolarization of the mitochondrial membrane initially occurred in response to fresh nZVI (≥ 40 min, 10 ppm) but was unaffected by its “aged” counterpart. (C) Intracellular ATP levels were measured with CellTiter-Glo. Significant reductions occurred in response to fresh nZVI (≥ 5 ppm, 3 h) “aged” nZVI (20 ppm, 3 h), and magnetite (20 ppm, 24 h). (D) Significant increases in caspase 3/7 activity occurred in response to fresh nZVI (≥ 10 ppm, 6 h and continued over the 24 h exposure). “Aged” nZVI also stimulated significant increases but at later time points. The lowest concentrations and earliest time points at which significant effects were recorded are marked by asterisks.

“aging” and surface modification of nZVI materials would modify their physical properties (agglomeration, iron content) and would differentially affect cell types (microglia) and neurons known to be OS-sensitive.

Materials and Methods

Five materials were used in this study: fresh (bare) nZVI, oxidized nZVI (“aged”), magnetite, and two surface-modified nZVI (SM-nZVI). The first SM-nZVI is a commercially available product (MRNIP) which is fresh nZVI modified with sodium polyaspartate (poly AA) (MW + 10,000 g/mol), and the second is fresh nZVI modified with the same polymer (poly-AA) but laboratory generated. This was done to ensure that the comparison between fresh bare nZVI and the SM-nZVI had the same underlying nZVI particle material because the manufacturing of MRNIP is proprietary. Both MRNIP and poly-AA particles behaved identically in this study. The sources of the various nZVI are described in the Supporting Information (SI) section. Concentration units were presented as “ppm” in keeping with toxicity nomenclature (1 ppm = 1 mg/L). The cell culture models, their maintenance, and exposure procedures have been fully described in the SI. The assays and methodologies for the physicochemical measures (iron (Fe^0) content, zeta potential, hydrodynamic diameter, and sedimentation) have been previously reported (18, 31) and are also described in the SI.

Results

OS and Microglia. Immortalized mouse microglia (BV2) were exposed to the various nZVI materials and major end points

of OS were measured (Figure 1A–D). Intracellular H_2O_2 generated from the oxidative burst was produced only in response to fresh nZVI (≥ 1 ppm, 30 min) and “aged” nZVI (≥ 10 ppm, 30 min) (Figure 1A). Both the commercial SM-nZVI (MRNIP) and the laboratory generated material (polyAA-nZVI) failed to stimulate the oxidative burst. Depolarization of the mitochondrial membrane, an index of apoptosis, occurred only in response to fresh nZVI (≥ 5 ppm, 40 min) (Figure 1B). Reductions of intracellular ATP, a marker of cellular viability, affected the microglia in the following rank order: fresh nZVI (5 ppm, 3 h) > “aged” nZVI (20 ppm, 3 h) > magnetite (20 ppm, 24 h) (Figure 1C). Increases in caspase 3/7 activity, an indicator of apoptosis, first occurred in response to fresh nZVI (≥ 10 ppm, 6 h) but also occurred at later exposures with “aged” nZVI (≥ 10 ppm, 18 h) (Figure 1D). SM-nZVI exposure failed to produce OS or apoptosis in these cells. Ultrastructurally, BV2 microglia exposed to fresh nZVI (5 ppm, 3 h) displayed large nZVI agglomerates housed in membrane-bound agglomerates (i.e., phagosomes) (Figure SI 1A). These inclusions were located in close proximity to populations of disrupted mitochondria. Light microscopy (LM) indicated that the nuclei of exposed BV2 (5 ppm, 6 h) were swollen and centrally located, which suggested apoptosis (Figure SI 1B).

Neurotoxicity. The response of N27 neurons to each nZVI material was examined with viability and morphological end points. Levels of intracellular ATP were reduced after a 6 h exposure in the following rank order: fresh nZVI (≥ 5 ppm, 1 h) > SM-nZVI (20 ppm, 1 h) > “aged” nZVI = magnetite (20 ppm, 6 h) (Figure 2). In contrast to the crisp, electron

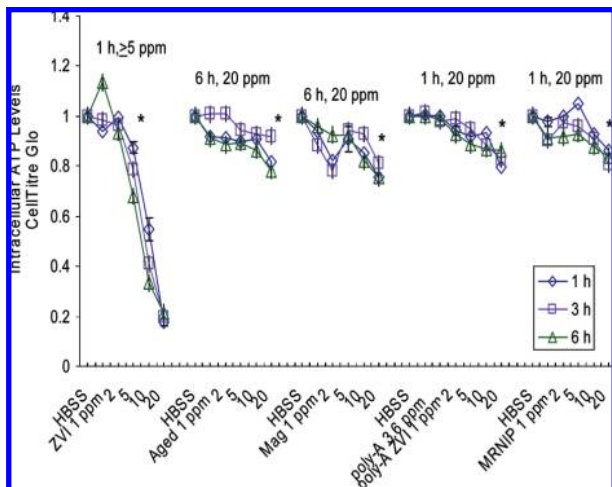


FIGURE 2. N27 neurons were exposed to 1–20 ppm of each material and levels of intracellular ATP levels were measured over a 6 h exposure with CellTiter-Glo. The following rank order of cytotoxicity was recorded: fresh nZVI (>5 ppm, 1 h) > Poly AA nZVI = MRNIP (20 ppm, 1 h) > “aged” nZVI (20 ppm, 6 h) = magnetite (20 ppm, 6 h). Asterisks mark the lowest concentration and earliest time points for significant responses.

dense appearance of nuclear chromatin seen ultrastructurally in control nuclei (Figure 3A), the nuclei and cytoplasm of N27 neurons exposed to fresh nZVI (1 ppm, 3 h) displayed a floccular material and a darkened, granular cytoplasm (Figure 3B). The nuclei and cytoplasm of N27 neurons treated

with either commercial or laboratory generated SM-nZVI (1 ppm, 3 h) appeared ultrastructurally normal. However, numerous examples of single particles and small agglomerates (~200–300 nm) of electron-dense nZVI appeared throughout and within the cell’s nuclei and mitochondria (Figure 3C). Evidence of electron-dense membrane invaginations, suggestive of clathrin-lined endocytotic vesicles (32, 33), was also noted in SM-nZVI treated neurons (Figure 3C and D, asterisks).

Particle Characterization. The Fe⁰ content of fresh nZVI, polyAA-nZVI, and MRNIP measured 35 ± 1%, 24 ± 1%, and 24 ± 2%, respectively. Reactivity tests with trichloroethylene indicated that they were all highly redox active. The half-life for nZVI’s conversion to iron oxides is approximately 3–6 months when stored in water at pH 10.6 (34). This was supported by the negligible iron content measured in the “aged” nZVI and magnetite materials. The surface charge (zeta potential) of the individual materials was influenced by the fluids in which they were exposed (Tables SI 1, SI 2, SI 3). For example, in HBSS, the zeta potentials ranged from –13.8 to –18.6 mV; in BV2 nutrient medium (Dulbecco’s Modified Eagle’s Medium, DMEM), they ranged from –7.1 to –10.1 mV, and in RPMI-1640, the media used to expose N27 neurons, they measured –8.0 to –13.3 mV. Although, the ionic strengths of HBSS, DMEM, and RPMI-1640 are similar (155, 166, and 151 mM, respectively), the particles measured in DMEM or RPMI had lower zeta potentials relative to the HBSS environment. This suggested that interactions occurred between the particle surface and the amino acids found in DMEM and RMPI (28).

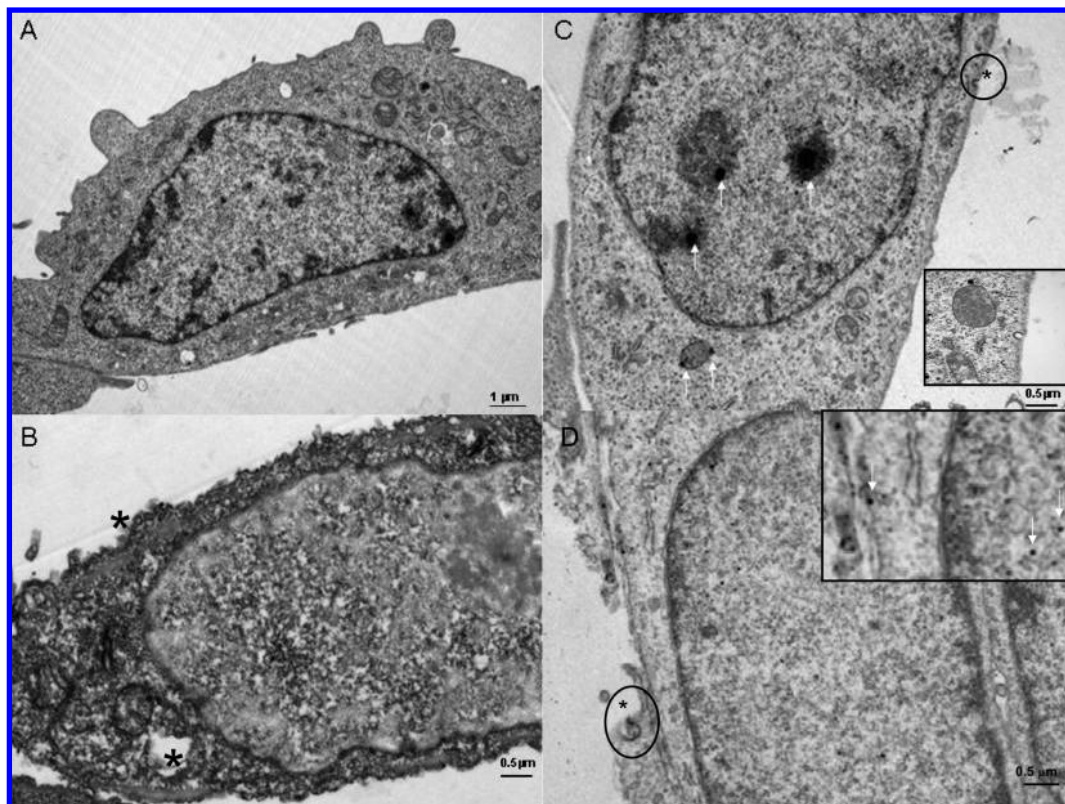


FIGURE 3. Nuclear chromatin of control N27 neurons displayed a high contrast appearance and ultrastructurally normal cytoplasm (Figure 3A). In contrast, the cytoplasm of N27 neurons exposed to fresh nZVI (1 ppm, 3 h) appeared darker and more condensed, and displayed a fibrillar material around the cell’s internal membrane (asterisks) and a perinuclear distribution of floccular material (Figure 3B). The cytoplasm of N27 neurons, treated with either laboratory-generated SM-nZVI (Figure 3C) or MRNIP (Figure 3D) (1 ppm, 3 h) appeared relatively normal ultrastructurally, although ZVI agglomerates (~200–500 nm) and single nanosize particles were noted in the nuclei and cytoplasm in response to both treatments (Figures 3 C and D, insert). Invaginations of the neuron’s cell membrane, suggestive of clathrin-lined endocytotic vesicles, were also noted in both SM-nZVI treated samples (Figure 3 C and D, circles, asterisks).

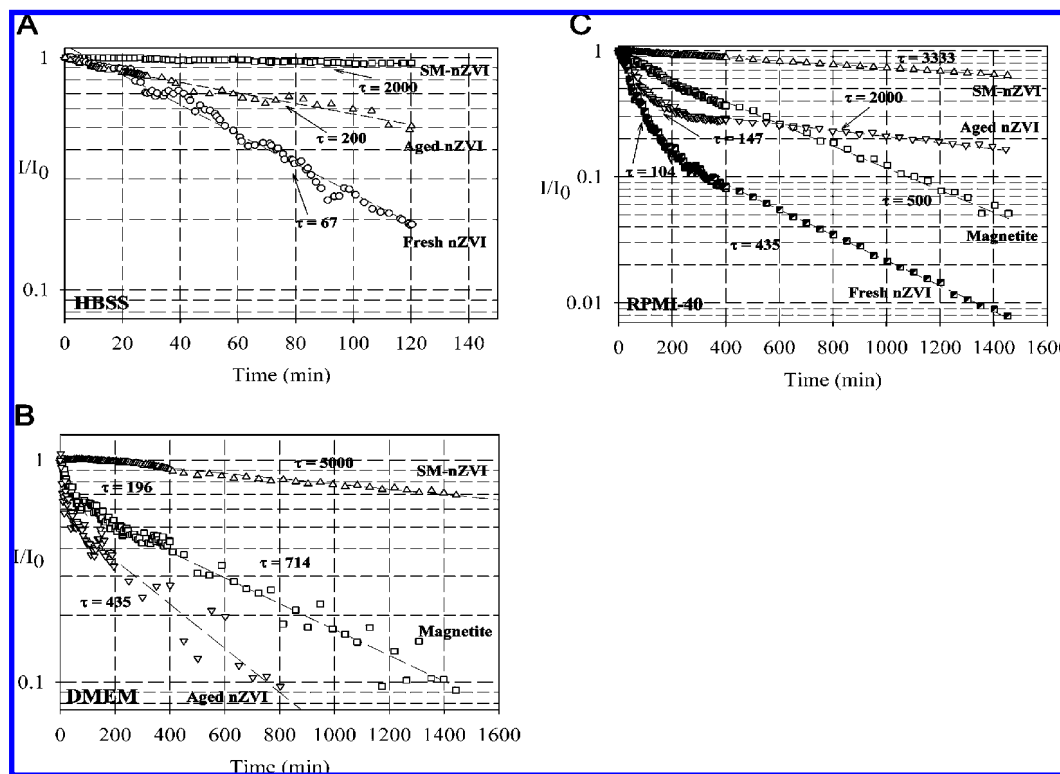


FIGURE 4. Sedimentation of fresh nZVI, “aged” nZVI, magnetite, and SM-nZVI (MRNIP) in (A) HBSS, (B) DMEM, and (C) RPMI. Sedimentation of fresh nZVI in DMEM (B) is not shown but behaved similarly to nZVI as shown in (C). Sedimentation of polyAA-nZVI was similar to MRNIP and their behavior is depicted by SM-nZVI.

Tables SI 1–SI 3 show the particle size distributions of the different nZVI materials under exposure conditions. For non-SM nZVI materials (i.e., fresh nZVI, “aged” nZVI, and magnetite), the size distributions were bimodal in all exposure vehicles, and contained both small (hydrodynamic radius, $R_H < 1 \mu\text{m}$) and large ($R_H > 2 \mu\text{m}$) agglomerates. The sedimentation of particles measured in each exposure vehicle (Figure 4A–C) indicated that fresh nZVI agglomerated and sedimented faster relative to the other materials. Over the 120 min recording period, the particle size distribution increased and then decreased as the larger agglomerates settled from the suspension, leaving behind the DSL-detectable smaller agglomerates.

The unmodified materials (fresh nZV, “aged”, magnetite) materials agglomerated rapidly as reported earlier (13). After 10 min, the agglomerate size (R_H) of each material was measured: fresh nZVI ($2.9 \mu\text{m}$), “aged” nZVI ($0.73 \mu\text{m}$), and magnetite ($0.53 \mu\text{m}$). These values related to the Fe^0 content of the material and suggested that the agglomerate size was influenced by the magnitude of the magnetic attraction between the particles (13). The agglomeration of SM-nZVI and MRNIP was much slower relative to the uncoated nZVI due to the electrosteric stabilization provided by the adsorbed polyAA (18). The same trends were observed for the agglomeration in DMEM and RPMI. The low sedimentation rate of SM-nZVI resulted from the reduced agglomeration of the coated particles although in HBSS the sedimentation ranking was similar. The agglomeration of polyAA-nZVI in HBSS, DMEM, and RPMI was not measured but was expected to behave identically to MRNIP because of their similar physical properties (e.g., Fe^0 content and polyAA coating).

Discussion

The present data show that nZVI materials (i.e., fresh, “aged”, and SM-nZVI) are differentially toxic to mammalian nerve cells. Interactions between nanoparticles and the biological

response of cells are thought to be influenced by the particle’s PC properties such as size, aggregation state, surface charge, and the presence of surface coatings (35, 36). Our data indicate that differences in bulk chemistry, “redox” activity surface chemistry, and sedimentation influenced the stimulation of OS in BV2 microglia and cytotoxicity in N27 neurons. In every instance, fresh nZVI was more toxic relative to its “aged”, oxidized, or surface-modified counterparts. In microglia, fresh nZVI stimulated high levels of ROS and caspase activity, reduced intracellular ATP levels, and depolarized the mitochondrial membrane at lower exposure times and concentrations relative to the other materials. The higher OS-mediated toxicity related to the higher iron content and “redox” activity of fresh nZVI. The relatively high iron content of fresh nZVI was expected since Fe^0 would have been largely oxidized in the “aged” and magnetite materials from corrosion by water. The OS response of “aged” nZVI could result from small amounts of ferrous ion present which could be further oxidized to ferric ion. Although it was not tested in the present study, nZVI’s high OS behavior could also relate to its ability to form free radicals in water (37, 38) and in exposure media (35). Fresh nZVI and SM-nZVI (both “redox” active) were also more cytotoxic to N27 neurons than “aged” nZVI and magnetite. Although, nZVI agglomerates were not seen in the cytoplasm of exposed N27 neurons, the presence of perinuclear floccular material and the rapid cytotoxicity in these cells indicated that they were adversely affected. Previous studies have reported that magnetite is toxic to rat liver cells (39) and lung cells (40), yet our data showed that it neither stimulated OS end points nor increased caspase 3/7 activity in BV2 microglia and was only marginally neurotoxic to N27 neurons. The low neurotoxicity of the oxidized materials correlated with their relatively low “redox” activity and is consistent with prior reports of Fe^0/Fe -oxide nanoparticles (38, 41) and other “redox”-active nanomaterials (42).

The influence of surface modification appeared to be cell-type-dependent. Although SM-nZVI had substantially more iron content relative to the “aged” nZVI or magnetite, surface coating appeared to reduce the OS response, suggesting an independent effect of the poly AA coating rather than the “redox” activity of these materials. The surface coating could alter the interaction of the particles with the BV2 cell membrane and phagocytosis or mitigate ROS production as reported (43, 44). In contrast, the presence of surface coating had less influence on nonphagocytic N27 toxicity which followed the order of “redox” activity (Fe⁰ content).

The poly AA surface coating affected agglomeration, surface charge, and the particle’s surface chemistry. This might affect its initial contact with the cell membrane and cellular intake process such as phagocytosis (microglia) or endocytosis (neurons). Agglomeration state would affect the actual process by which particles enter the cell. Although nanosize particles (1–100 nm) are smaller than the optimal size range (1–3 μm) for phagocytosis (45), the micron-size nZVI agglomerates could easily trigger BV2 microglia phagocytosis as demonstrated by the cell’s OS response and its ultrastructure. The agglomeration and subsequent sedimentation could also affect the exposure of the particles to cells in culture (46). For example, the higher toxicity of fresh nZVI materials to both BV2 microglia and N27 neurons might relate not only to its higher iron content and “redox” activity, but also to its faster agglomeration and sedimentation rate which would increase the amount and rate at which nZVI agglomerates physically contact the cells. Conversely, the surface coating of SM-nZVI minimized their agglomeration and sedimentation rate and limited their physical contact with the target cells. This possibility is suggested by the low OS response of BV2 exposed to SM-nZVI particles, in spite of their having an iron content relatively similar to that of fresh nZVI. Although, the smaller agglomerates remained largely suspended, some nanosize SM-nZVI particles did contact and enter the N27 neurons, as shown ultrastructurally. The inclusion of single and small agglomerates of SM-nZVI particles noted in the N27 neuronal cytoplasm and nuclei is noteworthy. The polymeric poly AA-surface coating of nZVI particles appeared to facilitate particle–cell interaction. Both the commercial (MRNIP) and laboratory-generated (polyAA-nZVI) particles were modified with polyaspartate. This biopolymer consists of aspartate units, a natural proteinogenic amino acid. Polymers have been used for controlled release formulations and drug-targeting systems (47) and polymeric surface modification using aspartate has been used to promote the delivery of nanosize particles to cells and tissues (48, 49). This may explain the presence of nanosize SM-nZVI particles inside the otherwise normal N27 neurons. Although no evidence of phagocytosis was seen, cellular entry of such nanosize materials through clathrin-lined caveoli, similar to that described by others (33, 50), was documented.

These results have important implications for using nZVI materials for groundwater remediation and for using surface coatings on these materials. The unmodified, relatively immobile nZVI particles oxidize in water and “age” over months into the nontoxic magnetite and/or maghemite (34) suggesting low risk to encountered ecosystems. Although surface modification increases nZVI’s dispersion, it also appears to decrease its toxicity. However, the poly AA surface modifier appeared to facilitate SM-nZVI’s cytoplasmic and nuclear entry into cells. This latter observation may have long-term biological consequences that are not evident over the limited exposure times of the present study. Since a variety of surface coatings which increase the mobility of nZVI in porous media (12, 14) are currently available, efforts should be made to fully characterize their toxicity.

Acknowledgments

We thank Dr. John Hong, National Institute of Environmental Health Sciences, RTP, NC for the BV2 and N27 immortalized cell lines. We also acknowledge the expert preparation of electron microscopy samples by Robert Bagnell, University of North Carolina, Chapel Hill, NC. Funding for the technical support of T.C.L. was provided by EPA Professional Service Contract EPO6D000663. Funding support for T.P. was provided by the Royal Thai Government and the Department of Defense (W912HQ-06-C-0038) and the U.S. EPA (R833326). This document has been reviewed by the National Health and Environmental Effects Research Laboratory and approved for publication. Approval does not signify that the contents reflect the views of the Agency, nor does mention of trade names or commercial products constitute the endorsement of recommendation for use.

Supporting Information Available

Information on the sources of the materials used in the study; the source and methodologies for the cultured cells used, their maintenance and exposures, and the various oxidative stress assays; descriptions of the various physicochemical assays used to measure iron (Fe⁰) content, zeta potential, hydrodynamic diameter, and sedimentation of the various materials are listed. One photograph (Figure SI 1A,B) documents the morphological response of nZVI exposed BV2 microglia. Three tables labeled SI 1, SI 2, and SI 3 describe the aggregation kinetics as hydrodynamic diameters and the sedimentation rate of the various materials in different exposure vehicles. This material is available free of charge via the Internet at <http://pubs.acs.org>.

Literature Cited

- (1) Zhang, W. X. Nanoscale iron particles for environmental remediation: an overview. *J. Nanopart. Res.* **2003**, *5*, 323–332.
- (2) Liu, Y.; Majetič, S. A.; Tilton, R. D.; Sholl, D. S.; Lowry, G. V. TCE dechlorination rates, pathways, and efficiency of nanoscale iron particles with different properties. *Environ. Sci. Technol.* **2005**, *39*, 1338–1345.
- (3) He, F.; Zhao, D. Manipulating the size and dispersibility of zerovalent iron nanoparticles by use of carboxymethyl cellulose stabilizers. *Environ. Sci. Technol.* **2007**, *41*, 6216–6221.
- (4) Lowry, G. V.; Johnson, K. M. Congener-Specific Dechlorination of Dissolved PCBs by Microscale and Nanoscale Zerovalent Iron in a Water/Methanol Solution. *Environ. Sci. Technol.* **2004**, *38*, 5208–5216.
- (5) Chiueh, C. C.; Rauhala, P. The redox pathway of S-nitrosoglutathione, glutathione and nitric oxide in cell to neuron communications. *Free Radical Res.* **1999**, *31*, 641–650.
- (6) Ponder, S. M.; Darab, J. G.; Mallouk, T. E. Remediation of Cr(VI) and Pb(II) aqueous solutions using supported, nanoscale zerovalent iron. *Environ. Sci. Technol.* **2000**, *34*, 2564–2569.
- (7) Houch, L.; Mack, E. J.; Hydutsky, B. W.; Hershman, J. M.; Skluzacek, J.; Mallouk, T. E. Carbothermal synthesis of carbon-supported nanoscale zero-valent iron particles for the remediation of hexavalent chromium. *Environ. Sci. Technol.* **2008**, *42*, 2600–2605.
- (8) Liu, Y. Q.; Choi, H.; Dionysiou, D.; Lowry, G. V. Trichloroethene hydrodechlorination in water by highly disordered monometallic nanoiron. *Chem. Mater.* **2005**, *17*, 5315–5322.
- (9) Limbach, L. K.; Wick, P.; Manser, P.; Grass, R. N.; Brumink, A.; Stark, W. J. Exposure of engineered nanoparticles to human lung epithelial cells: influence of chemical composition and catalytic activity on oxidative stress. *Environ. Sci. Technol.* **2007**, *41*, 4158–4163.
- (10) Li, X. Q.; Zhang, W. X. Iron nanoparticles: the core-shell structure and unique properties for Ni(II) sequestration. *Langmuir* **2006**, *22*, 4638–4642.
- (11) Henn, K. W.; Waddill, D. W. Utilization of nanoscale zero-valent iron for source remediation - a case study. *Remediation J.* **2006**, *16*, 57–77.
- (12) Saleh, N.; Sirk, K.; Liu, Y.; Phenrat, T.; Dufour, B.; Matyjaszewski, K.; Tilton, R. D.; Lowry, G. V. Surface modifications enhance nanoiron transport and NAPL targeting in saturated porous media 3695. *Environ. Eng. Sci.* **2007**, *24*, 45–57.

- (13) Phenrat, T.; Saleh, N.; Sirk, K.; Tilton, R. D.; Lowry, G. V. Aggregation and sedimentation of aqueous nanoscale zerovalent iron dispersions. *Environ. Sci. Technol.* **2007**, *41*, 284–290.
- (14) Saleh, N.; Kim, H.-J.; Phenrat, T.; Matyjaszewski, K.; Tilton, R. D.; Lowry, G. V. Ionic strength and composition affect the mobility of surface-modified NZVI in water-saturated sand columns. *Environ. Sci. Technol.* **2008**, *42*, 3349–3355.
- (15) Schrick, B.; Hydutsky, B. W.; Blough, J. L.; Mallouk, T. E. Delivery vehicles for zerovalent metal nanoparticles in soil and groundwater. *Chem. Mater.* **2004**, *16*, 2187–2193.
- (16) Saleh, N.; Phenrat, T.; Sirk, K.; Dufour, B.; Ok, J.; Sarbu, T.; Matyjaszewski, K.; Tilton, R. D.; Lowry, G. V. Adsorbed triblock copolymers deliver reactive iron nanoparticles to the oil/water interface. *Nano Lett.* **2005**, *5*, 2489–2494.
- (17) He, F.; Zhao, D. Y.; Liu, J. C.; Roberts, C. B. Stabilization of Fe-Pd nanoparticles with sodium carboxymethyl cellulose for enhanced transport and dechlorination of trichloroethylene in soil and groundwater. *Ind. Eng. Chem. Res.* **2007**, *46*, 29–34.
- (18) Phenrat, T.; Saleh, N.; Sirk, K.; Kim, H.; Tilton, R.; Lowry, G. V. Stabilization of aqueous nanoscale zerovalent iron dispersions by anionic polyelectrolytes: adsorbed anionic polyelectrolyte layer properties and their effect on aggregation and sedimentation. *J. Nanoparticle Res.* **2008**, *10*, 795–814.
- (19) Kanel, S.; Goswami, R. R.; Clement, T. P.; Barnett, M. D.; Zhao, D. Two dimensional transport characteristics of surface stabilized zero-valent iron nanoparticles in porous media. *Environ. Sci. Technol.* **2008**, *42*, 896–900.
- (20) Kreyling, W. G.; Semmler, M.; Erbe, F.; Mayer, P.; Takenaka, S.; Schulz, H.; Oberdorster, G.; Ziesenis, A. Translocation of ultrafine insoluble iridium particles from lung epithelium to extrapulmonary organs is size dependent but very low. *J. Toxicol. Environ. Health, A* **2002**, *65*, 1513–1530.
- (21) Lockman, P. R.; Kozlira, J. M.; Mumper, R. J.; Allen, D. D. Nanoparticle surface charges alter blood-brain barrier integrity and permeability. *J. Drug Target.* **2004**, *12*, 635–641.
- (22) Fariss, M. W.; Chan, C. B.; Patel, M.; Van Houten, B.; Orrenius, S. Role of mitochondria in toxic oxidative stress. *Mol. Interv.* **2005**, *5*, 94–111.
- (23) Block, M. L.; Zecca, L.; Hong, J. S. Microglia-mediated neurotoxicity: uncovering the molecular mechanisms. *Nat. Rev. Neurosci.* **2007**, *8*, 57–69.
- (24) Shafer, L. L.; McNulty, J. A.; Young, M. R. Brain activation of monocyte lineage cells: brain-derived soluble factors differentially regulate BV2 microglia and peripheral macrophage immune functions. *Neuroimmunomodulation* **2002**, *10*, 283–294.
- (25) Kang, J.; Yang, M.; Jou, I.; Joe, E. Identification of protein kinase C isoforms involved in interferon-gamma-induced expression of inducible nitric oxide synthase in murine BV2 microglia. *Neurosci. Lett.* **2001**, *299*, 205–208.
- (26) Chang, R. C.; Rota, C.; Glover, R. E.; Mason, R. P.; Hong, J. S. A novel effect of an opioid receptor antagonist, naloxone, on the production of reactive oxygen species by microglia: a study by electron paramagnetic resonance spectroscopy. *Brain Res.* **2000**, *854*, 224–229.
- (27) Long, T. C.; Saleh, N.; Tilton, R. D.; Lowry, G. V.; Veronesi, B. Titanium dioxide (P25) produces reactive oxygen species in immortalized brain microglia (BV2): implications for nanoparticle neurotoxicity. *Environ. Sci. Technol.* **2006**, *40*, 4346–4352.
- (28) Zhou, W.; Hurlbert, M. S.; Schaack, J.; Prasad, K. N.; Freed, C. R. Overexpression of human alpha-synuclein causes dopamine neuron death in rat primary culture and immortalized mesencephalon-derived cells. *Brain Res.* **2000**, *866*, 33–43.
- (29) Sama, P.; Long, T. C.; Hester, S.; Tajuba, J.; Parker, J.; Chen, L. C.; Veronesi, B. The Cellular and genomic response of an immortalized microglia cell line (BV2) to concentrated ambient particulate matter. *Inhalation Toxicol.* **2007**, *19*, 1079–1087.
- (30) Veronesi, B.; Makwana, O.; Pooler, M.; Chen, L. C. Effects of subchronic exposures to concentrated ambient particles. VII. Degeneration of dopaminergic neurons in Apo E-/- mice. *Inhalation Toxicol.* **2005**, *17*, 235–241.
- (31) Long, T. C.; Tajuba, J.; Sama, P.; Saleh, N.; Swartz, C.; Parker, J.; Hester, S.; Lowry, G. V.; Veronesi, B. Nanosize titanium dioxide stimulates reactive oxygen species in brain microglia and damages neurons *in vitro*. *Environ. Health Perspect.* **2007**, *115*, 1631–1633.
- (32) Chithrani, B. D.; Chan, W. C. Elucidating the mechanism of cellular uptake and removal of protein-coated gold nanoparticles of different sizes and shapes. *Nano Lett.* **2007**, *7*, 1542–1550.
- (33) Harush-Frenkel, O.; Debotton, N.; Benita, S.; Altschuler, Y. Targeting of nanoparticles to the clathrin-mediated endocytic pathway. *Biochem. Biophys. Res. Commun.* **2007**, *353*, 26–32.
- (34) Liu, Y.; Lowry, G. V. Effect of particle age (Fe⁰ content) and solution pH on NZVI reactivity: H₂ evolution and TCE dechlorination. *Environ. Sci. Technol.* **2006**, *40*, 6085–6090.
- (35) Power, K. W.; Palazuelos, M.; Moudgil, B. M.; Roberts, S. M. Characterization of the size, shape, and state of dispersion of nanoparticles for toxicological studies. *Nanotoxicology* **2007**, *1*, 42–51.
- (36) Nel, A.; Xia, T.; Madler, L.; Li, N. Toxic potential of materials at the nanolevel. *Science* **2006**, *311*, 622–627.
- (37) Joo, S. H.; Feitz, A. J.; Waite, T. D. Oxidative degradation of the carbothioate herbicide, molinate, using nanoscale zero-valent iron. *Environ. Sci. Technol.* **2004**, *38*, 2242–2247.
- (38) Lee, C.; Kim, J.; Lee, W.; Nelson, K. L.; Yoon, J.; Sedlak, D. L. Bactericidal effect of zero-valent iron nanoparticles on *Escherichia coli*. *Environ. Sci. Technol.* **2008**, *42* (13), 4927–4933.
- (39) Hussain, S. M.; Hess, K. L.; Gearhart, J. M.; Geiss, K. T.; Schlager, J. J. In vitro toxicity of nanoparticles in BRL 3A rat liver cells. *Toxicol. In Vitro* **2005**, *19*, 975–983.
- (40) Karlsson, H. L.; Nilsson, L.; Moller, L. Subway particles are more genotoxic than street particles and induce oxidative stress in cultured human lung cells. *Chem. Res. Toxicol.* **2005**, *18*, 19–23.
- (41) Wiesner, M. R.; Lowry, G. V.; Alvarez, P.; Dionysiou, D.; Biswas, P. Assessing the risks of manufactured nanomaterials. *Environ. Sci. Technol.* **2006**, *40*, 4336–4345.
- (42) Adams, L. K.; Lyon, D. Y.; Alvarez, P. Comparative eco-toxicity of nanoscale TiO₂, SiO₂, and ZnO water suspensions. *Water Res.* **2006**, *40*, 3527–3532.
- (43) Tong, Z.; Bischoff, M.; Nies, L.; Applegate, B.; Turco, R. Impact of fullerene (C60) on a soil microbial community. *Environ. Sci. Technol.* **2007**, *41*, 2985–2991.
- (44) Lyon, D. Y.; Brunet, L.; Hinkal, G. W.; Wiesner, M. R.; Alvarez, P. J. J. Antibacterial activity of fullerene water suspensions (nC60) is not due to ROS-mediated damage. *Nano Lett.* **2008**, *8*, 1539–1543.
- (45) Tabata, Y.; Ikada, Y. Effect of the size and surface charge of polymer microspheres on their phagocytosis by macrophage. *Biomaterials* **1988**, *9*, 356–362.
- (46) Limbach, L. K. K.; Li, Y. C.; Grass, R. N.; Brunner, T. J.; Hintermann, M. A.; Muller, M.; Gunther, D.; Stark, W. J. Oxide nanoparticle uptake in human lung fibroblasts: effects of particle size, agglomeration, and diffusion at low concentrations. *Environ. Sci. Technol.* **2005**, *39*, 9376.
- (47) Qiu, L. Y.; Bae, Y. H. Polymer architecture and drug delivery. *Pharm. Res.* **2006**, *23*, 1–30.
- (48) Hara, K.; Tsujimoto, H.; Huang, C. C.; Kawashima, Y.; Mimura, H.; Miwa, N. The effect of poly(aspartic acid-co-lactic acid) nanospheres on the lung metastasis of B16BL6 melanoma cells by intravenous administration. *Oncol. Rep.* **2006**, *16*, 1215–1220.
- (49) Arimura, H.; Ohya, Y.; Ouchi, T. Formation of core-shell type biodegradable polymeric micelles from amphiphilic poly(aspartic acid)-block-poly(lactide) diblock copolymer. *Biomacromolecules* **2005**, *6*, 720–725.
- (50) Mayor, S.; Pagano, R. E. Pathways of clathrin-independent endocytosis. *Nat. Rev. Mol. Cell Biol.* **2007**, *8*, 603–612.

ES801955N